



LAWRENCE
LIVERMORE
NATIONAL
LABORATORY

Effect of Fluoride Ions on the Anodic Behavior of Mill Annealed and Aged Alloy 22

Martin A. Rodriguez, Ricardo M. Carranza-, Raul B. Rebak

October 17, 2003

Corrosion/2004
New Orleans, LA, United States
March 28, 2004 through April 1, 2004

Disclaimer

This document was prepared as an account of work sponsored by an agency of the United States Government. Neither the United States Government nor the University of California nor any of their employees, makes any warranty, express or implied, or assumes any legal liability or responsibility for the accuracy, completeness, or usefulness of any information, apparatus, product, or process disclosed, or represents that its use would not infringe privately owned rights. Reference herein to any specific commercial product, process, or service by trade name, trademark, manufacturer, or otherwise, does not necessarily constitute or imply its endorsement, recommendation, or favoring by the United States Government or the University of California. The views and opinions of authors expressed herein do not necessarily state or reflect those of the United States Government or the University of California, and shall not be used for advertising or product endorsement purposes.

09October2003

Paper04700tobepresentedattheNACEInternational,CORROSION/04ConferenceinNewOrleans,
LA28Marchto01April2004

EFFECT OF FLUORIDE IONS ON THE ANODIC BEHAVIOR OF MILL ANNEALED AND THERMALLY AGED ALLOY 22

Martín A. Rodríguez and Ricardo M. Carranza
Inst. Sabato and Dep. Materiales, Comisión Nacional de Energía Atómica
Av. Gral. Paz 1499
B1650 KNA San Martín, Buenos Aires, ARGENTINA

Raúl B. Rebak
Lawrence Livermore National Laboratory
7000 East Ave, L-631
Livermore, CA 94550, USA

ABSTRACT

Alloy 22 (N06022) is the current candidate alloy to fabricate the external wall of the high level nuclear waste containers for the Yucca Mountain repository. It was of interest to study and compare the general and localized corrosion susceptibility of Alloy 22 in saturated NaF solutions (~ 1 M NaF) at 90°C. Standard electrochemical tests such as cyclic potentiodynamic polarization, amperometry, potentiometry, and electrochemical impedance spectroscopy were used. Studied variables included the solution pH and the alloy microstructure (thermal aging). Results show that Alloy 22 is highly resistant to general and localized corrosion in pure fluoride solutions. Thermal aging is not detrimental and even seems to be slightly beneficial for general corrosion in alkaline solutions.

Keywords: N06022, fluoride, pitting corrosion, crevice corrosion, transpassivity, thermal aging, cyclic polarization, EIS, corrosion rate, nuclear waste disposal

INTRODUCTION

Worldwide, geological repository has been considered as the ultimate home for high-level nuclear waste by many countries. In the United States, Yucca Mountain is the designated site to bury approximately 70,000 tons of high-level nuclear wastes in specially engineered packages.¹ These packages are designed to maintain isolation of the waste for a minimum of 10,000 years and the containers will be double-walled cylinders. The inner wall must provide mechanical strength and the outer wall is the corrosion

corrosion resistant barrier. The current design specifies Type 316 (S31603) nuclear grade (NG) stainless steel for the inner container and Alloy 22 (N06022) for the outer container.^{2 3} The waste container should not leak radioactive material for at least 10,000 years. If water is present in the repository site, it is assumed that Alloy 22 may undergo three different corrosion mechanisms, namely, (1) General or uniform corrosion, (2) Localized corrosion and (3) Stress corrosion cracking.⁴ This paper discusses only the first two types of degradation.

Due to the heat generated by the radioactive decay of the waste, the containers might experience temperatures as high as 180°C during the first 1000 years after emplacement. The maximum allowed temperature by design specifications is 350°C.¹ Studies of the thermal stability of Alloy 22 for such a long time are impractical in the laboratory. Extrapolation of the thermal aging data is required to predict the alloy behavior over the 10,000 years life. Previous studies have shown that the mechanical and corrosion properties of this alloy did not change when it was aged for up to 40,000 h at 427°C.^{5 6 7} Microstructural changes that occur in the base material and welds have been evaluated at temperatures from 427 to 760°C. Tetrahedral close packed (TCP) phases precipitate in Alloy 22 at temperatures of 593°C and higher.^{8 9 10} These phases could have a detrimental effect upon corrosion resistance and cause a loss of mechanical ductility. A long range ordering reaction (LRO) can occur at lower temperatures and produces an ordered Ni₃(Cr,Mo) phase.^{7 8 11} This ordering reaction is thought to cause little or no effect on corrosion and causes only a slight loss in ductility.

Many commercial nickel alloys are useful in various applications because of passive oxide films that form naturally on their surfaces. However, such passive films are often susceptible to breakdown by mechanisms of pitting and crevice corrosion. This type of attack specially occurs in the presence of halide compounds.^{12 13} Different quantities of fluorides and chlorides can be naturally found in ground waters. While the effects of chloride on the passive state and localized corrosion have been studied extensively, the effects of other compounds such as fluorides have not been fully characterized.¹⁴

It has been reported by several authors that nickel-based alloys generally have high resistance to corrosion in fluoride solutions.^{15 16 17} In recent studies the results demonstrated that some nickel alloys containing chromium, molybdenum, and tungsten have shown an excellent resistance to pitting and crevice corrosion in sodium fluoride solutions at different temperatures.^{14 18}

The aim of this study was to investigate the effects of pH and alloy thermal aging in ~1 M NaF solutions on the corrosion behavior of Alloy 22, both at the open circuit potential and in the passive and transpassive domains.

EXPERIMENTAL PROCEDURE

The Alloy 22 specimens were prepared from wrought mill annealed plate stock (MA probes). The chemical composition of the alloy in weight percent was 59.20% Ni, 20.62% Cr, 13.91% Mo, 2.68% W, 2.80% Fe, 0.01% Co, 0.14% Mn, 0.002% C, and 0.0001% S. Some samples were aged for 10 h at 760°C (TCP probes) and 1000 h at 538°C (LRO probes). Aging was performed in air and the samples were quenched in water after the heat treatment. Parallel piped specimens measuring 12 mm x 12 mm x 15 mm were mounted with a PTFE compression gasket (ASTM G5).¹⁹ A torque was applied to the gasket to ensure a leak-proof assembly. The occluded area from the PTFE gasket was 0.75 cm² and the exposed area of the sample was 10.5 cm². The samples had a finished grinding of abrasive paper number 600 and were degreased in acetone and washed in distilled water 1 hour prior to testing.

Electrochemical measurements were conducted in a three-electrode, borosilicate glass cell. A water-cooled condenser combined with a water trap was used to maintain solution concentration and controlled atmosphere. The solution temperature was controlled by immersing the cell in a thermostated water bath. The cell was equipped with both an air-cooled Luggin and a saturated calomel electrode.

trode (SCE) reference. A large area platinum wire was used as counter electrode. The electrochemical tests were carried out in room temperature saturated NaF solutions (these solutions are approximately 1 M NaF) at pH values of 6, 7.3 and 9. The naturally prepared 1 M NaF has a pH of approximately 9. To adjust the pH to lower values, small amounts of HF were added. The test temperature was 90°C.

The cyclic potentiodynamic polarization technique (ASTM G 61) ¹⁹ was used to determine the electrochemical characteristics and susceptibility to localized corrosion of Alloy 22 in these media. The potential scan was started 150 mV below the corrosion potential versus the reference electrode. The scan rate used was 0.167 mV/s, and the scan direction was reversed when the current reached 10 mA/cm². At the conclusion of the test, the specimens were examined microscopically for signs of corrosion. Amperometry measurements were conducted at two selected potentials in the passive and transpassive domains. Specimens were held potentiostatically at 0.000 and 0.370 V_{SCE} for a 2 hours period while the anodic current density was recorded. A cathodic treatment at -1.000 V_{SCE} for 5 minutes was performed previously to the tests. Before immersing the testing specimens, the solutions were purged for half an hour with nitrogen inert gas and it was maintained during the tests. Electrochemical Impedance Spectroscopy (EIS) measurements were carried out at the corrosion potential and at a potential of 0.100 V_{SCE}. A 5 mV amplitude sinusoidal potential signal was superimposed to the corrosion potential of the test probe. The frequency scan was started at 10 kHz and ended at 1 mHz. The parameters of equivalent circuit mathematical models were fitted to these data in order to obtain polarization resistances R_p , which led to instantaneous uniform corrosion rates. The Tafel constants, β_A and β_C , were assumed to be ± 0.12 V/decade for the calculation of the corrosion currents from R_p values.

Corrosion rates were recalculated using Equation (1)

$$CR (\text{mm/yr}) = \frac{K i_{\text{corr}} EW}{\rho} \quad (1)$$

Where i_{corr} is the passive corrosion current density in A/cm², EW is the equivalent weight, K is the faradaic conversion factor (3,270 mmg A⁻¹ cm⁻¹ yr⁻¹) and ρ is the density in g/cm³ (8.69 g/cm³ for Alloy 22). Assuming congruent dissolution of the major alloying elements as Ni²⁺, Cr³⁺, Mo³⁺, Fe³⁺, and W⁴⁺ the EW for Alloy 22 is 23.28.²⁰

Solutions and precipitates obtained after cyclic polarization measurements were analyzed using X Ray Fluorescence (XRF). The technique used was Total Reflection X-Ray Fluorescence (TRXF), which involves very low incident angles. These low angles allow the x-rays to undergo total reflection. This minimizes the adsorption of the x-rays and greatly enhances the lower limits of detection. This allows very accurate determinations of metallic cations. The lamp used in the analysis was equipped with a molybdenum anode hindering the presence of this element in the analysis. The amount of total metal cations found both in solutions and precipitates were expressed as mol of cations per volume of initial solution.

RESULTS AND DISCUSSION

Cyclic polarization

Figures 1-3 show typical cyclic polarization curves for Alloys 22 in nitrogen purged solutions. Corrosion potential did not show a clear dependence with either the pH or the microstructure (the metallurgically aged condition). For the lowest tested pH values, a small activation current peak was always observed which was rarely found at pH 9 (Fig. 1). Alloy 22 presented a wide passive range with approximately constant passive current density. The passive current density increased as the pH decreased (Fig. 1), but

it was independent of the microstructure (Fig. 2). Passive current values for different pH and microstructures are listed in Table 1. The decrease in pH values from 9 to 6 produced an increase both in passive and transpassive current densities.

At potentials higher than those corresponding to the passive zone an abrupt increase of current took place with the formation of a transpassive current peak. This transpassive peak could be deconvoluted in at least three gaussian peaks as can be seen in Figure 5. Both potential and current peak maxima increased with decreasing pH, indicating that the electrochemical reactions that produce these peaks are pH dependent in a magnitude of around 50 mV per pH unit (Fig. 4). All nickel oxides (including $\text{Ni}(\text{OH})_2$) would present a similar behavior (59 mV per pH unit) according to thermodynamic data.²¹ Chromium dissolution to chromate or dichromate would present higher pH dependences.²¹ In simulated concentrated water (SCW) at pH 11 and 60°C and 90°C, results of coordinated polarization experiments and passive film analyses indicated that the pronounced anodic oxidation peak between 200 and 400 mV_{SCE} was due to the oxidation of Mo^{4+} to Mo^{6+} within the passive film.²² Thermodynamic data predict, as for chromium, larger pH dependence for this reaction in molybdenum.

After this first transpassive peak, a second current increase took place in the polarization curves (second transpassivity). This second current increase seemed to be pH dependent but in a lesser extent than the first transpassive multiple peak. The potential scan was reversed once the anodic current reached 1 to 10 mA·cm⁻² (the maximum anodic current attained before potential scan reversal was increased at pH 6 to allow full visualization of the first transpassive peak). A large current hysteresis between forward and reverse potential scans was observed. Once the polarization curve was finished a yellowish gelatinous precipitate was found in the solution inside the electrochemical cell and partially covering the probe. The cyclic polarization was then repeated but reversing the scan at potentials immediately after the first transpassive peak (Fig. 3). Neither precipitates nor positive current hysteresis were found this time, on the contrary, the electrode seemed to be completely passivated in the reverse potential scan.

Microscopic observation

At the conclusion of all the polarization curves, the specimens were examined microscopically for signs of corrosion. Neither pits nor crevices were found in any case. Positive current hysteresis observed in the cyclic polarization curves should then be attributed to film dissolution and to the corresponding loss of corrosion protective power.

X-Ray Fluorescence (XRF)

A qualitative analysis of the precipitates found indicated the presence of significant amounts of silicon (Si) and Ni as main components. The most likely source of dissolved Si is the borosilicate test cell. Amorphous silica has a great adsorption capacity and can trap heavy metal ions in its structure.²³ Both solutions and precipitates, obtained after the polarization curves were ended, were analyzed quantitatively looking for metal ions using XRF. Figure 6 shows the concentrations found after polarization curves of Figure 3. Ni, Cr, Fe and W were the principal elements found in the analysis. It must be taken into account that a certain amount of Ni could have been deposited in the counter electrode because of the nobility of this element, and consequently it did not appear in this analysis. As it was previously mentioned, the presence of Mo was hindered by the molybdenum anode used in the equipment, so that the anodic charge calculated with these metallic element concentrations was lower than that obtained by integration of the anodic current during the wider cyclic polarization. From Figure 3 it is seen that a significant metal dissolution had occurred after the first transpassive peak reinforcing the idea that this peak corresponds to solid phase transformation from one oxidation state to another with higher oxidation state. Possibly, the same oxide presents three different reversible potentials for different surface states. Mo dissolution at the first transpassive peak, as proposed elsewhere²², could not be evaluated

dissolution at the first transpassive peak, as proposed elsewhere²², could not be evaluated because Mo cannot be detected in these tests.

Potentiometry

The analysis of the localized corrosion susceptibility with the electrochemical parameters extracted from the cyclic polarization curves was carried out, anyway, following the procedure of a previous publication.¹⁴ The corrosion resistance model for the degradation of the waste package specifies that the outer wall may suffer localized corrosion only above a certain critical potential (E_{crit}). This E_{crit} represents a potential above which the current increases substantially and irreversibly above the passive current density. At a potential below E_{crit} , the corrosion rate will be given by the passivated dissolution rate at the respective value of the free corroding potential (E_{corr}). E_{crit} is a parameter that may vary in value depending on the testing method. This parameter could represent, for example, the breakdown potential (E_b) or a repassivation potential (E_r). In any case, the safety margin against localized corrosion is given by $\Delta E = E_{crit} - E_{corr}$. Since the true value of E_{crit} is not known, another criterion is used to establish a threshold potential. The threshold potential is defined as E_{20} and represents the lowest value of potential during potentiodynamic polarization at which the current density reached $20 \mu A/cm^2$. This predetermined current density could have been attained through an intermediary anodic peak (as in this case), the onset of pitting corrosion, crevice corrosion or even by transpassivity. Therefore, the criterion used in this study is considered as a “highly conservative value” since the intermediary anodic peaks may not represent steady state conditions.

In order to determine $\Delta E = E_{20} - E_{corr}$, the open circuit potential attained after 24 h immersion in fresh solutions without nitrogen purging were measured as a function of pH and microstructure, results are shown in Table 2. Even in the case that the first transpassive peak, which determined the E_{20} value, would diminish the corrosion resistance of the passive film, the safety margin ΔE was high enough to prevent from corrosion degradation, under the supposition that E_{corr} after 24 h can be extrapolated to longer times. The shift of the corrosion potentials after immersion until 24 h was approximately 350 mV, a value that is in good agreement with published results for longer periods. Results obtained at Lawrence Livermore National Labs for as long as four years indicate a shift in more than 500 mV in corrosion potential for other solutions.²²

Amperometry

Figure 7 shows the variation of the anodic current when two different constant potentials, one in the passive range and the other at the top of the first transpassive peak, were applied to MA coupons of Alloy 22 immersed in saturated NaF solutions at pH 9 purged with nitrogen. After the tests the probe held potentiostatically at the passive potential showed a metallic characteristic aspect while the probe held at the transpassive potential showed interference colors. After two hours the currents of passive and transpassive potentials were quite similar compared with the corresponding values obtained during cyclic polarization (Fig. 3) where the difference between them was of two orders of magnitude. This is in good agreement with the results obtained when the potential scan was reversed immediately after the first transpassive peak (Fig. 3) and with the idea that this peak corresponds to an homogeneous solid electrochemical reaction.

Electrochemical Impedance Spectroscopy

The corrosion rate of freely corroding samples was monitored using the Electrochemical Impedance Spectroscopy Technique. Figures 8 and 9 show typical Bode diagrams obtained during EIS measurements at the corrosion potential. A diagram like that of Figure 8 was obtained immediately after

immersion of the samples and when the corrosion potential was at the small anodic activation peak potential range. It was observed that the phase angle presented two maxima corresponding to two time constants. The high frequency time constant was attributed to exchange current densities due to the proximity to the reversible potentials for the metal oxidation. The low frequency time constant is then considered as the charge transfer leading to the corrosion rate. Once the anodic oxide was formed and the corrosion potential was moved towards the full passive range, impedance diagrams changed to simpler ones presenting a single time constant as that shown in Figure 9. In both cases Bode plots presented phase angle maxima smaller than 90° and absolute values of the impedance modulus slope lower than 1. Correspondingly, Nyquist plots (not shown) showed a depressed semi-circle aspect. Many reasons have been proposed in the literature to explain this behavior such as surface roughness, frequency dispersion of time constants due to local inhomogeneities in the dielectric material, porosity mass transport effects and relaxation effects.^{24 25 26 27} In order to account for these effects, non-ideal capacitors must be introduced into the equivalent circuit proposed to reproduce the experimental results, according to the theory presented by Jonscher.²⁸ In the present case, equivalent circuits consisting of a pure resistance R_Ω in series with parallel circuits of ideal resistances and non-ideal capacitors called constant phase elements $(R_\Omega - R \parallel CPE)^{24}$ were proposed. These equivalent circuits are the simplest ones that can simulate adequately the experimental results and are depicted in Figure 10. They do not include all the complexities involved in taking into account the exact semiconductor properties of the metallic oxides which could imply to add more complex circuit elements as diodes²⁹ or frequency dependent resistances typical of porous electrodes with distributed resistances and capacitances in a network.²⁴ For the proposed equivalent circuits, the following transfer functions are obtained:

$$Z_\omega = R_\Omega + \frac{R_{LF}}{1 + (j\omega R_{LF} C_{LF})^{\beta_{LF}}} \quad (2)$$

for one phase angle maximum, and

$$Z_\omega = R_\Omega + \frac{R_{HF}}{1 + (j\omega R_{HF} C_{HF})^{\beta_{HF}}} + \frac{R_{LF}}{1 + (j\omega R_{LF} C_{LF})^{\beta_{LF}}} \quad (3)$$

for two phase angle maxima, where j is the imaginary unit ($\sqrt{-1}$), ω is the angular frequency, R_Ω is the ohmic component of the complex impedance Z_ω at very high frequencies, C denotes ideal capacitors, β is the dispersion parameter indicating the deviation of the model from pure $R-C$ circuits²⁸ and subscripts LF and HF correspond to the parameters fitted at low and high frequencies, respectively.

Equations 2 and 3 were fitted to the experimental impedance spectra using the Simplex method with software developed in our laboratory. A good agreement was obtained between fitted and experimental results as can be shown from Figures 8 and 9.

Impedance measurements were made periodically at the corrosion potential during 24 hours of immersion. Using the above mentioned methodology fitting parameters were obtained and the low frequency ones are shown in Figure 11 for Alloy 22 in MA condition at pH 9 as an example. It can be seen that the passivation of the alloy is associated with an increase in the low frequency resistance R_{LF} and a decrease of the low frequency capacitance C_{LF} . The values obtained for C_{LF} lie in the double layer capacitance domain (between 20 to 50 $\mu F \cdot cm^{-2}$). When the initial E_{corr} was located at potentials in the active anodic peak range, high values of C_{LF} were obtained indicating the presence of faradic processes which could produce pseudo-capacitances higher than the double layer capacitance. As was mentioned before the low frequency resistance R_{LF} was associated, then, to the transfer resistance leading to the corrosion current and it will be mentioned hereafter as the polarization resistance R_p .

Figure 12 shows the variation of both E_{corr} and R_p as a function of time. The variation of R_p with time can be associated to both a change in E_{corr} (shifting to more noble potentials with time) and to the elapsed time at a fixed potential, which produces increasing and/or aging of the oxide film.

Figure 13 shows the variation of R_p and corrosion rate, calculated with eq. 1, as a function of the pH of the solution and the microstructure of the alloy after 24 h of immersion. It can be seen that, for all the microstructures in the range of pH tested, the corrosion rate calculated was very low, and that it decreased when the pH was increased. There were no differences in corrosion rates for the three microstructures at pH 6 but at pH 9 lower corrosion rates were obtained for the aged samples being LRO the one that presented the lowest corrosion rate at this pH. Long-range ordering reaction is thought to cause detrimental effects upon stress corrosion cracking and hydrogen embrittlement but no or little effect upon passivity.²² The presence of tetrahedral close packed (TCP) phases precipitates not only did not increase corrosion rate but also decrease this parameter at pH 9. These differences in corrosion behavior for different microstructures were not detected by passive currents differences in the cyclic polarization curves possibly due to the potential scan rate used. At pH 9 lower corrosion rates implies higher periods of time to wait until stationary state is reached. Steady state polarization curves will surely detect these differences in corrosion behavior.

CONCLUSIONS

- Alloy 22 is highly resistant to localized corrosion in saturated NaF solutions at 90°C for the three microstructures used: MA, TCP and LRO. Neither pits nor crevices were found after anodic polarizations reaching currents up to 10 mA cm^{-2} . Positive current hysteresis observed in cyclic polarization curves are due to film dissolution.
- Solution pH showed a considerable influence over passive and transpassive currents for the three microstructures studied. The lower the pH the higher the passive and transpassive current densities.
- The first transpassive peak observed in the anodic potential scans should be attributed to electrochemical transformations within the oxide like those of nickel and/or molybdenum.
- General corrosion rates for all microstructures, tested after 24 h immersion in saturated NaF solutions at 90°C in the pH range between 6 and 9, are very low, $0.4 \mu\text{m year}^{-1}$ and lower. At the higher pH LRO and TCP microstructures have lower corrosion rates than the MA condition.
- Degradation of corrosion properties by the presence of TCP phases was not detected in the studied conditions.

ACKNOWLEDGMENTS

This work was performed under the auspices of the U. S. Department of Energy (DOE) by the University of California Lawrence Livermore National Laboratory under contract N° W-7405-Eng-48. This work is supported by the Yucca Mountain Project, which is part of the Office of Civilian Radioactive Waste Management (OCRWM).

REFERENCES

- 1 Yucca Mountain Science and Engineering Report, U.S. Department of Energy, Office of Civilian Radioactive Waste Management, DOE/RW -0539, Las Vegas, NV, May 2001. l-
- 2 Civilian Radioactive Waste Management, System Management and Operating Contractor, "Update to the EIS Engineering File for the Waste Package in Support of the final EIS," Civilian Radioactive Waste Management System, System Management and Operating Contractor, TDR EBS-MD-000010, Revision 00, ICN01, Las Vegas, NV, 2000. p-a-
- 3 Civilian Radioactive Waste Management, System Management and Operating Contractor, "Uncanistered Spent Nuclear Fuel Disposal Container System Description Document," Civilian Radioactive Waste Management System, System Management and Operating Contractor, SDD UDC-SE-000001, Revision 01, ICN01, Las Vegas, NV, 2000. -
- 4 R.B. Rebak and J.C. Estill, "Review of Corrosion Modes for Alloy 22 Regarding Lifetime Expectancy of Nuclear Waste Containers", Paper II.4.1, Volume 757, Fall Meeting of the Materials Research Society in Boston (MA), 2 -6 December 2002. x-
- 5 R. B. Rebak, in Proceedings of the Symposium on Passivity and its Breakdown, The Electrochemical Society, Volume 97 -26, pp. 1001- 1012 (1998). o-
- 6 A.K. Roy, D.L. Flemin g, B. Y. Lum, MP, March, pp. 54 (1998)
- 7 R.B. Rebak and N.E. Koon, Paper 153, Corrosion/98, NACE International, Houston (1998).
- 8 M. Raghavan, B.J. Berkowitz, J.C. Scanlon, Met. Trans., 13A, 979 (1982).
- 9 M.J. Cieslak, T.J. Headley and D. Romig Jr., Metall. Trans., 17A, 2035 (1986).
- 10 H.M. Tawancy, J. Mater. Sci., 31, 3929 (1996).
- 11 F. G. Hodge and H.S. Ahluwalia, Proceedings of the 12th International Corrosion Congress, Houston, TX, NACE International, 5B (1993) p. 4031.
- 12 Z. Szklarska -Smialowska, Pitting Corrosion of Metals, NACE International, Houston, TX (1989).
- 13 B.F. Brown, J. Kruger and R. W. Staehle, Localized Corrosion, NACE International, Houston, TX (1986).
- 14 N.S. Meck, P. Crook, S.D. Day, and R. B. Rebak, Paper 03682, Corrosion/03 NACE International, 2003, Houston, Texas. a-
- 15 G.H. Koch, Localized Corrosion in Halides Other than Chlorides, MTI Publication 41, Materials Technology Institute of the Chemical Process Industries, Inc., Columbus, Ohio, Published by NACE International (1995).
- 16 G.H. Koch, N.G. Thompson and J.L. Means, Effect of Trace Elements in Flue Gas Desulfurization Environments on the Corrosion of Alloys - A literature Review, EPRI Report CS -4374 (Palo Alto, CA: EPRI, 1986).
- 17 G.H. Koch, G. W. Kistler and W. Mirich, Evaluation of Flue Gas Desulfurization Materials in Mixing Zone: R. D. Morrow, Sr., Generating Station, EPRI Report CS -5476 (Palo Alto, CA: EPRI 1987).
- 18 N.S. Meck, P. Crook and R.B. Rebak in Corrosion Science, A Retrospective and Current Status in Honor of Robert P. Frankenthal, PV 2002 -13, pp. 355 -368, The Electrochemical Society, Pennington, NJ, 2002.
- 19 Annual Book of ASTM Standards, Volume 03.02, American Society for testing and Materials, West Conshohocken, PA (2001).
- 20 American Society for Testing and Materials. G102 -89. Standard Practice for Calculation of Corrosion Rates and Related Information from Electrochemical Measurements. Annual Book of Standards. West Conshohocken, PA: American Society for Testing and Materials: 416 -422, 1999.

21. Atlas of Electrochemical Equilibria in Aqueous Solutions, Marcel Pourbaix, NACE, Houston, Texas, USA, c.1974, p.333.
22. Waste Package Material Performance Peer Review Panel, Las Vegas, Nevada, United States Department of Energy, 2002.
23. I.M. Kolthoff, E.B. Sandell, E.J. Meehan and S. Bruckenstein - Análisis Químico Cuantitativo - Librería y Editorial Nigar S.R.L., Buenos Aires, Cuarta Edición, 1972.
24. J.R. Macdonald, Impedance Spectroscopy, John Wiley (1987).
25. K. Jüttner, W.J. Lorenz and W. Paatsch, Corrosion Sci. **29**, 2279 (1989)
26. W. Scheider, J. Phys. Chem. **79**, 127 (1975)
27. W.J. Lorenz, M.W. Kendig and F. Mansfeld, J. Electrochem. Soc. **135**, 332 (1988)
28. A.K. Jonscher, Phys. Stat. Sol. A. **32**, 665 (1975).
29. M.M. Loherengel, J.W. Shcultze and H.D. Speckman, Electrochim. Acta **31**, 123 (1986).

TABLE 1
PASSIVE CURRENT DENSITIES FOR ALLOY 2219 NS AT 90°C.
AVERAGED VALUE FROM CYCLIC POTENTIODYNAMIC POLARIZATION CURVES IN THE
PASSIVE RANGE.

	$i_{\text{PASSIVITY}}, \mu\text{m}/\text{cm}^2$		
pH	MA	TCP	LRO
6	2,02	2,15	2,07
7,3	0,87	-	-
9	0,65	0,60	0,71

TABLE 2
SAFETY MARGIN FOR TRANS PASSIVITY ONSET FOR ALLOY 2219 NS AT 90°C.

	$E_{20} - E_{\text{CORR}}(24\text{hs}), \text{V}$		
pH	MA	TCP	LRO
6	0,407	0,391	0,459
7,3	0,425	-	-
9	0,456	0,401	0,385

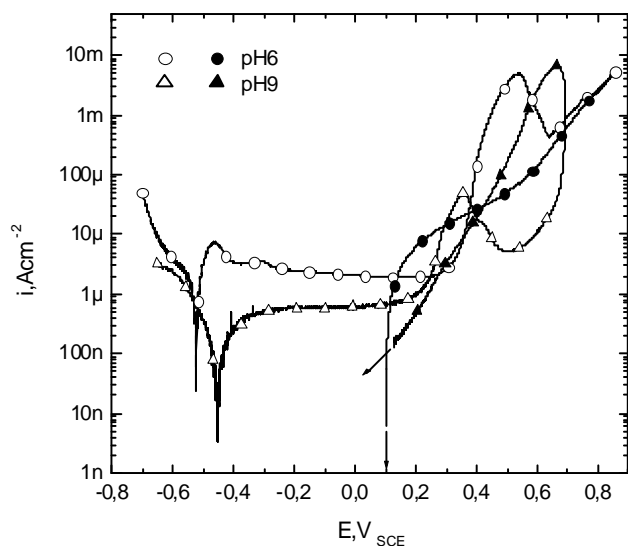


FIGURE 1 – Cyclic potentiodynamic polarization curves for Alloy 22 TCP in sat. NaF at 90°C. Scan rate 0.167 mV/s, N₂ bubbling. Empty symbols: direct scan, full symbols: reverse scan.

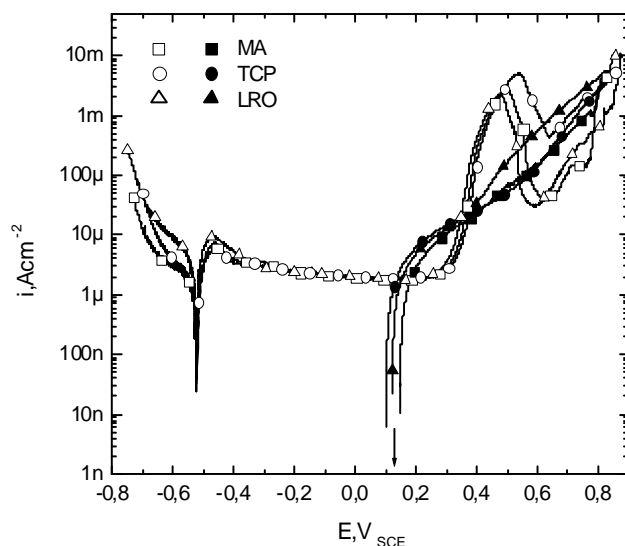


FIGURE 2 – Cyclic potentiodynamic polarization curves for Alloy 22 in sat. NaF, pH 6 at 90°C. Scan rate 0.167 mV/s, N₂ bubbling. Empty symbols: direct scan, full symbols: reverse scan.

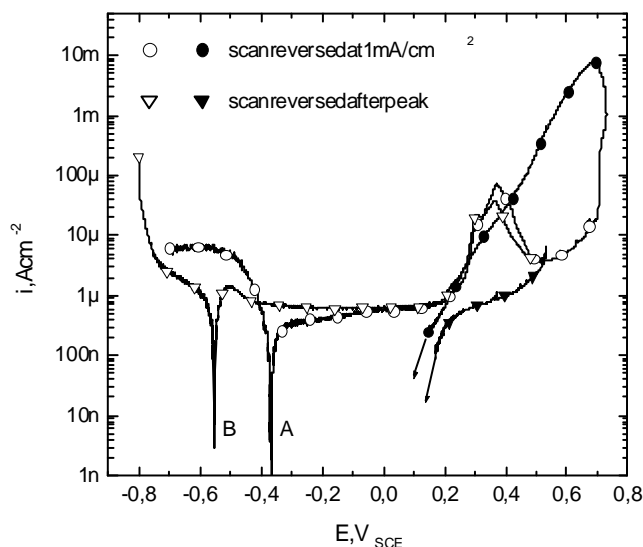


FIGURE 3 – Cyclic potentiodynamic polarization curves for Alloy 22 MA in sat. NaF, pH 9 at 90°C. Scan rate 0.167 mV/s, N₂ bubbling. Empty symbols: direct scan, full symbols: reverse scan.

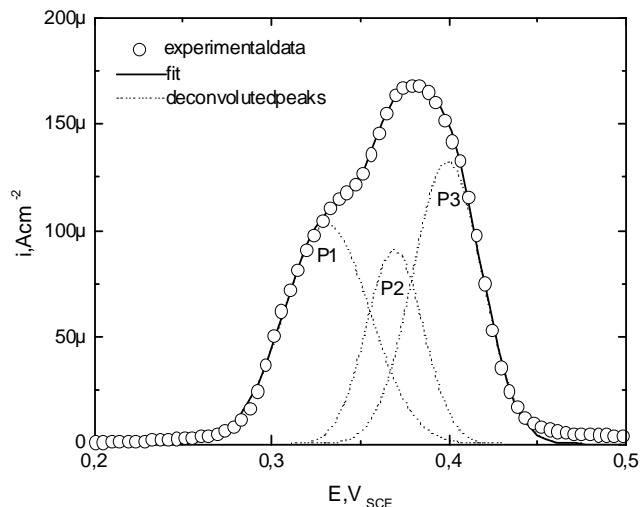


FIGURE 5 - Current density vs. potential plot for Alloy 22 LRO in sat. NaF, pH 9 at 90°C. Scan rate 0.167 mV/s, N₂ bubbling. P1: peak number 1, P2: peak number 2, P3: peak number 3.

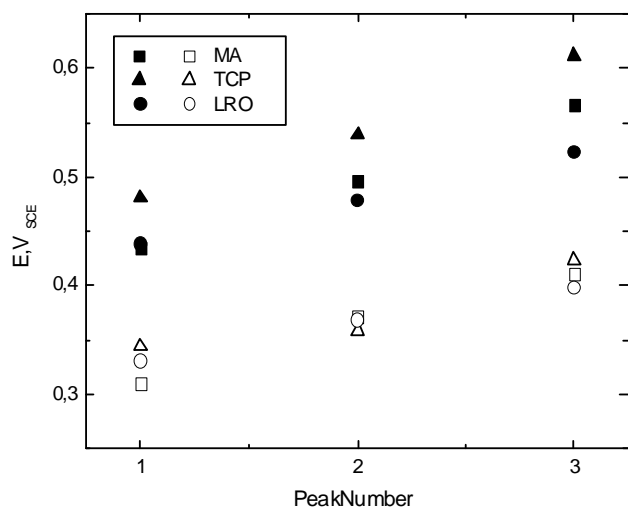


FIGURE 4 – Deconvoluted peak potentials of the first transpassive peak for Alloy 22 in sat. NaF at 90°C. Empty symbols: pH 9, fully bubbled; filled symbols: pH 6.

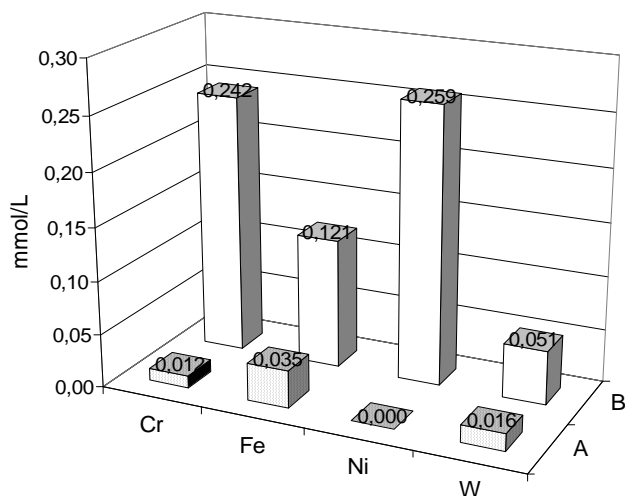


FIGURE 6 – Concentration of dissolved metal ions for Alloy 22 MA in sat. NaF, pH 9 at 90°C corresponding to cyclic potentiodynamic polarization curves A and B of Figure 3.

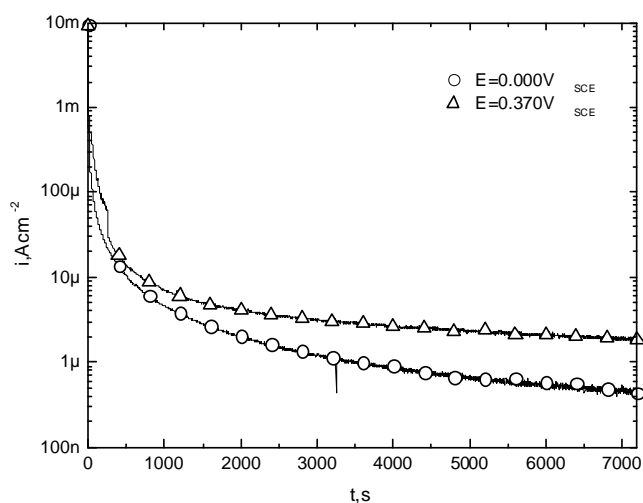


FIGURE 7 – Amperometry for Alloy 22 MA in sat. NaF, pH 9 and 90°C. N₂ bubbling.

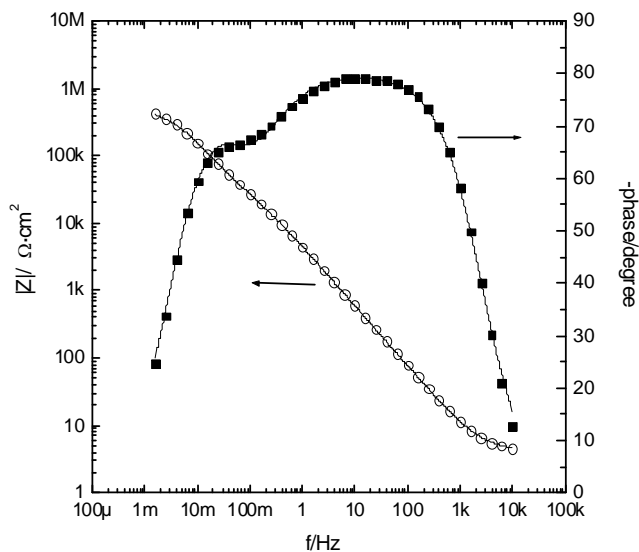


FIGURE 8 – Bode plot for Alloy 22 MA in sat. NaF, pH 7.3, 90°C, at $E_{corr} = -0.516V_{SCE}$, after 5h of immersion, without N₂ bubbling.

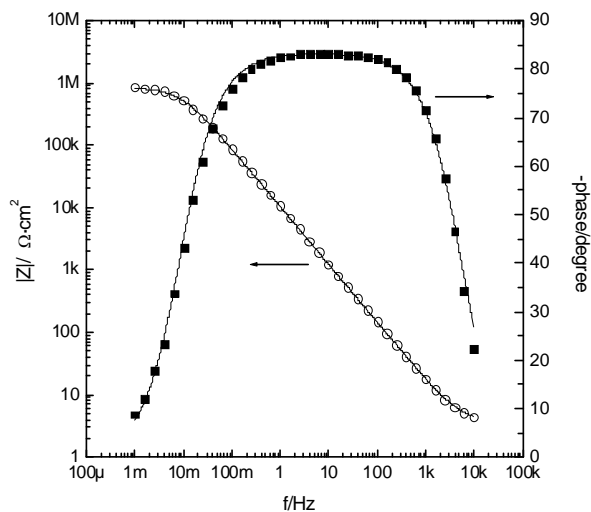
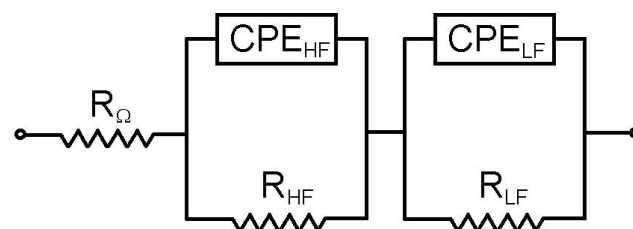


FIGURE 9 – Bode plot for Alloy 22 MA in sat. NaF, pH 7.3, 90°C, at $E_{\text{corr}} = -0.112 \text{ V}_{\text{SCE}}$, after 24 hours of immersion, without N_2 bubbling.

a - two time constants



b- single time constant

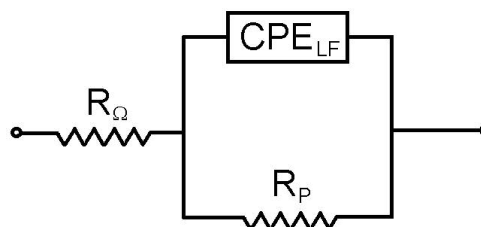


FIGURE 10 – Equivalent Circuits fitted to the experimental impedance results like those of Figures 8 and 9 respectively

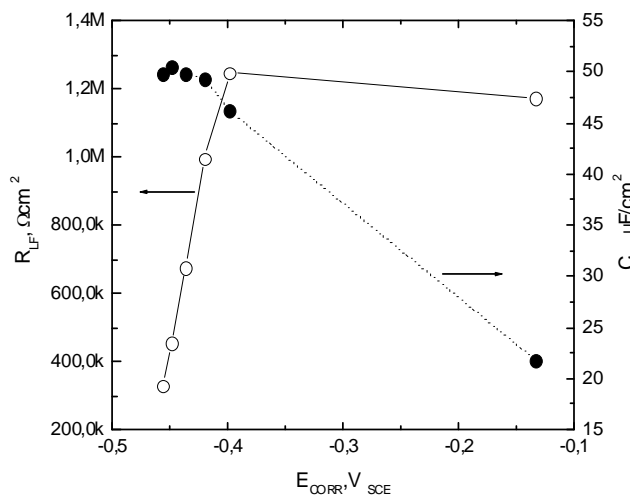


FIGURE 11 – Variation of R_{LF} and C_{LF} with E_{corr} for Alloy 22 MA in sat. NaF, pH 9 at 90°C, without N_2 bubbling.

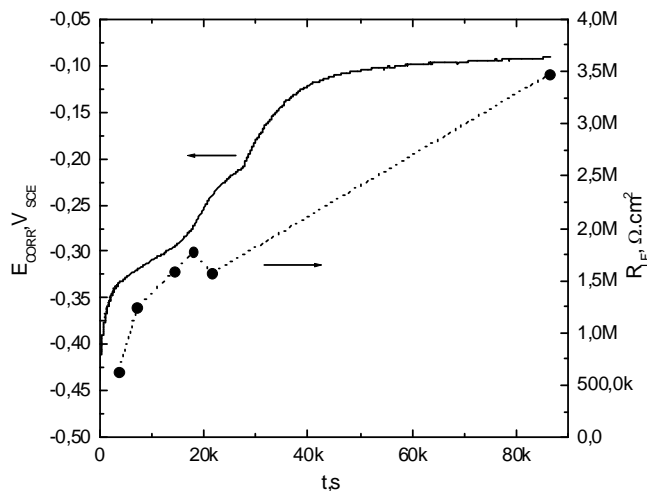


FIGURE 12 – Corrosion potential and low frequency resistance for Alloy 22 TCP in sat. NaF, pH 9 at 90°C, without N_2 bubbling.

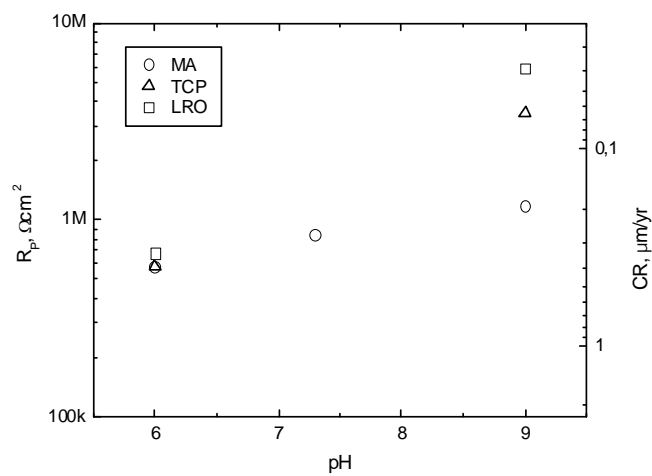


FIGURE 13 – Variation with pH of polarization resistances and corrosion rates for Alloy 22 in sat. NaF at 90°C after 24 h of immersion, without N₂ bubbling.